Separation Science and Technology
Publication details, including instructions for authors and subscription information:
http://www.informaworld.com/smpp/title~content=t713708471

Fouling Control in a Submerged Flat Sheet Membrane System: Part II—Two-Phase Flow Characterization and CFD Simulations

N. V. Ndinisa[a]; A. G. Fane[b]; D. E. Wiley[b]; D. F. Fletcher[c]
[a] Department of Chemical Engineering, Durban Institute of Technology, Durban, South Africa [b] UNESCO Centre for Membrane Science and Technology, University of New South Wales, NSW, Australia [c] Department of Chemical Engineering, University of Sydney, NSW, Australia

To cite this Article Ndinisa, N. V. , Fane, A. G. , Wiley, D. E. and Fletcher, D. F.(2006) 'Fouling Control in a Submerged Flat Sheet Membrane System: Part II—Two-Phase Flow Characterization and CFD Simulations', Separation Science and Technology, 41: 7, 1411 — 1445
To link to this Article: DOI: 10.1080/01496390600633915
URL: http://dx.doi.org/10.1080/01496390600633915

Separation Science and Technology, 41: 1411–1445, 2006

ISSN 0149-6395 print/1520-5754 online
DOI: 10.1080/01496390600633915

Fouling Control in a Submerged Flat Sheet Membrane System: Part II—Two-Phase Flow Characterization and CFD Simulations

N. V. Ndinisa
Department of Chemical Engineering, Durban Institute of Technology, Durban, South Africa

A. G. Fane and D. E. Wiley
UNESCO Centre for Membrane Science and Technology, University of New South Wales, NSW, Australia

D. F. Fletcher
Department of Chemical Engineering, University of Sydney, NSW, Australia

Abstract: Gas-liquid two-phase flow has been shown to be very effective in reducing fouling for different membrane modules with different feeds, including submerged flat sheet membranes used in membrane bioreactors for treatment of wastewater. Although gas-liquid two-phase flow occurring on the lumen side of tubular or hollow-fiber membranes has been very well characterized the two-phase flow regime in submerged membrane processes is different to that inside external membranes. Characterization of two-phase flow in submerged flat sheet membrane modules has not been previously reported and hence the use of two-phase flow in these modules has not yet been optimized. This paper reports on characterization of two-phase flow for a submerged flat sheet membrane module with the aim of identifying the most effective flow profiles for fouling minimization. In order to

Received 12 January 2006, Accepted 5 February 2006
Address correspondence to A. G. Fane, UNESCO Centre for Membrane Science and Technology, University of New South Wales, NSW 2052, Australia. E-mail: a.fane@unsw.edu.au

better understand the fouling control process by two-phase flow, CFD simulations were also conducted. It was found experimentally that an increase in the bubble size leads to an increase in the cleaning effect, however, for bubbles larger than the channel gap between the submerged flat sheet membranes, any further increase in the bubble diameter had only a minor effect on the cleaning process. CFD simulations revealed that flux enhancement was primarily due to an increase in the overall shear stress on the membrane and to more turbulence generated by introduction of the gas phase.

Keywords: Gas-liquid two-phase flow, fouling reduction, submerged flat sheet membrane bioreactor, membrane baffles, wastewater treatment, CFD simulations

INTRODUCTION

The use of membrane bioreactors (MBRs) for wastewater treatment is increasing. Essentially MBRs involve coupling of a biological reactor (mostly aerobic) with a membrane separation system, thus eliminating the need for a secondary settling tank. Such a combination offers several advantages over conventional wastewater treatment methods, such as small footprint plant (1), high quality effluent (2), an increase in the organic loading (3) and a lower rate of sludge production (4). In coupling a membrane system with a bioreactor, the membrane can either be placed external to the bioreactor or be directly immersed in the bioreactor. The majority of commercial MBRs currently use an immersed membrane which is mostly either a hollow fiber or a flat sheet membrane module (5). Membrane fouling due to concentration polarization, which lowers the permeate flux, is still a major factor hindering faster commercialization of the MBR processes.

Among the different ways to enhance the flux in ultrafiltration and microfilatration membrane processes, air sparging has recently been shown to be effective in combating fouling for different kinds of feed solutions. Air sparging consists of generating an unsteady flow by injecting air into the concentrate stream. A gas-liquid two-phase flow is then obtained in the feed compartment. The relative motion of the liquid and gaseous phases are thought to create hydrodynamic unsteadiness in the feed channel, which limits formation of the concentration boundary layer and thus minimizes membrane fouling. Air sparging has been shown to be very efficient for flux enhancement with hollow fiber membranes for different kinds of solid-liquid suspensions, for example for synthetic suspensions containing bacterial cells (6), dextran and albumin (7), and clays (8). Air sparging has also been shown to enhance flux in tubular membranes, for example, for solid-liquid suspensions like clay suspensions (9) and for solutions containing macromolecules like dextran, or mixtures of blue dextran and BSA (10). Although few studies have been reported for flat sheet membranes, gas-liquid two-phase flow was found to enhance flux in the ultrafiltration and

microfiltration of bacterial suspensions using organic flat sheet membranes (6) and for baker's yeast suspensions using ceramic membranes (11).

Most of the studies which have evaluated gas-liquid two-phase flow as a flux enhancing mechanism have been conducted on processes where the gas-liquid two-phase flow occurs on the lumen side of the membrane and therefore the permeate flows from the inside to the outside, that is, "in-to-out" filtration. However, as noted earlier, most MBRs make use of a submerged membrane so that bubbling occurs on the outside of the membrane and the filtration mode is "out-to-in." As a result a different pattern of two-phase flow can be expected for submerged membranes compared with external membranes. For "in-to-out" filtration systems, particularly tubular and hollow fiber systems, characterization of two-phase flow in the membrane modules has been thoroughly conducted in order to identify characteristics of two-phase flow that are responsible for enhancing flux (12). Of all the different regimes of two-phase flow, slug flow has been found to be the most effective regime in combating fouling (12). Slug flow is an intrinsically complex flow pattern due to its inherent unsteadiness. It consists of long bubbles that are almost as large as the tube diameter and these bubbles are separated by liquid plugs which sometimes may contain small dispersed bubbles. These bubbles are usually referred to as Taylor bubbles. Between the Taylor bubbles and the tube wall a small liquid falling film exists and shear stresses in this film have been found to be very high (13, 14). Also the wake of the Taylor bubbles is turbulent thus creating unsteadiness which may help prevent formation of a concentration boundary layer.

In our previous paper (15) we have identified the conditions at which gas-liquid two-phase flow is effective in reducing fouling for a submerged membrane system. However, characterization of two-phase flow in these systems has not been reported. The mechanisms by which two-phase flow enhances flux in submerged membrane systems may be different to that at work in external membrane systems. For example, with a submerged flat sheet membrane, slug flow may not be the dominant flow regime. Therefore there is a need to characterize two-phase flow for submerged membrane systems in order to identify the characteristics that are responsible for flux improvement. In this study, characterization of gas-liquid two-phase flow was conducted for a submerged flat sheet membrane. In order to better understand the fouling reduction process, CFD simulations were performed to obtain an insight into the two-phase flow profile and distribution of shear stress on the membrane surface. Although CFD investigations of two-phase flow inside tubular membrane have been performed by Taha and Cui (13), no such simulations have been conducted for submerged flat sheet membranes. This is the first study that reports on the characterization of two-phase flow in submerged flat membranes and presents complementary CFD simulations. Such information is vital for the optimization of the gas-liquid two-phase flow fouling control.

MATERIALS AND METHODS

Two-phase flow characterization

The experimental set-up is similar to that described in our previous paper (15). The position of the diffuser and the membrane in the tank are shown in Fig. 1. The process feed tank for the investigations of this study was filled with clean Milli-Q water instead of the yeast suspension used in our previous paper. Although the presence of the yeast particles in the filtration experiment may, to a certain extent, influence the behavior of the gas bubbles (16), it has been assumed that this influence is not very significant. The use of a particle-free environment was also required because we relied on images of the two-phase flow which could not be obtained when the yeast suspension was used as the bubbles became obscured. A Nikon Coolpix995 digital camera, positioned about 30 cm from the feed tank was used to take digital images and to record short 40 second movies of the two-phase flow pattern.

The main activity involved recording pictures with a digital camera under different conditions. The desired set of nozzles was fitted to the tank and involved circular nozzles of diameters 0.5, 1.0, 1.5 and 2.0 mm. After fitting the nozzles, the feed tank was filled with pure Milli-Q water. The membrane module was then inserted into the tank and secured. The air blower was switched on and the desired air flow rate selected in the range

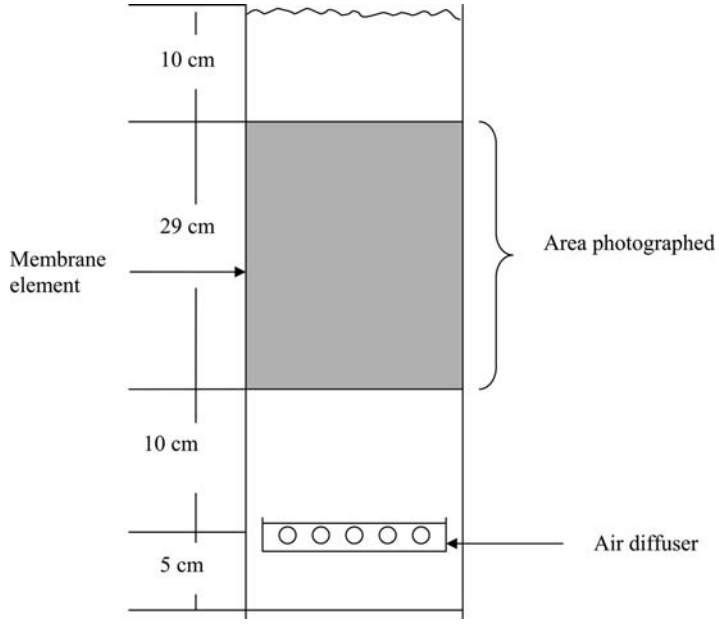

Figure 1. Illustration of the setup showing the area photographed for analysis.

2, 4, 6, and 8 l/min (similar to the yeast filtration experiments). Numerous pictures were taken with the digital camera and then downloaded to a PC using Nikon software. The digital pictures were originally in black and white JPEG format and had to be transformed into grayscale TIFF format using Adobe Photoshop before they could be processed further. The pictures were then analysed using AnalySIS® software. For each picture analyzed, the software produced information such as the total number of bubbles, the surface area of each bubble, the mean diameter of the bubble and the perimeter of each bubble.

CFD Simulations

An Eulerian two-fluid model was used to simulate two-phase flow conditions similar to those encountered in the experimental study. In this model, the continuous (liquid) and the dispersed (gas bubbles) phases are considered in an Eulerian representation and the model is based on mass and momentum balances for each phase, obtained over a volume within which the fluid can be treated as a continuum mixture. The basic description of this model, including the governing equations, have been presented elsewhere (14). Only additional information required for these simulations that was not included previously, is detailed here. The two-fluid model treats each fluid as a continuum having its own velocity field and occupying the whole domain, with the presence of each fluid represented using a volume fraction. The model allows a slip velocity to exist between the liquid and the gas phases. This model is mostly used for cases where the bubble size is smaller than the grid size, as it is based on volume averaged equations. The flow conditions inside the channel are expected to be predominantly turbulent since the introduction of the gas makes the transition from laminar to turbulent to occur sooner (13). The standard two equation k-ε turbulence model was used to account for turbulence in the liquid phase and the zero-equation dispersed phase model is used to account for turbulence in the gas-phase. The Sato particle-induced turbulence correction is used in order to model the extra turbulence created by the presence of the bubbles (17). The drag force has been modeled via the Grace correlation, which takes into account the fact that as the bubbles become larger, their shape changes, first to ellipsoidal and then to spherical cap, resulting in a volume fraction dependent drag coefficient (17). The turbulence dispersion force, which arises because of the liquid phase turbulence action on the bubbles, is estimated using the model of Lopez de Bertodano (18).

The geometry used for the simulations was identical to that used for the experiments (Fig. 1) with the exception that for the simulations only half of the tank was created with the membrane plane used as a symmetry plane since similar hydrodynamic conditions were expected to prevail on both sides of the membrane. In another set of simulations, baffles were created in the gap between the membrane and the wall. The baffles were used in the experiments

and shown to improve the distribution of air across the membrane surface and hence to improve the uniformity of the wall shear stress (15). In the experiments, a fixed number of baffles were used (13 baffles), whereas in the CFD simulations different numbers of baffles were tested in order to understand the effect of the baffles on the overall wall shear stress and to establish an optimal number of baffles. Fig. 2 shows a typical geometric setup containing 13 baffles.

Simulation Conditions

The governing equations were solved using the commercial CFD code, CFX 5.6 from ANSYS. This code solves the conservation equations using a finite volume method. For the Eulerian simulations described in this section, a three-dimensional structured grid was generated using CFX Build. The grid was non-uniform and consisted of 42 cells (across the vessel height) × 43 cells (across the vessel width) × 8 cells (across the vessel depth). A fine enough grid was chosen to achieve grid independent results. An example of the grid used is shown in Fig. 3. The grid size was biased, with cells expanding with height in the region above the membrane. This was done because this area is above the membrane and the flow pattern in that region is of little interest.

The flow was assumed to be transient. The fluids were water and air at 293 K and were assumed to be incompressible and isothermal and to have constant fluid properties. For all walls and the membrane, the boundary

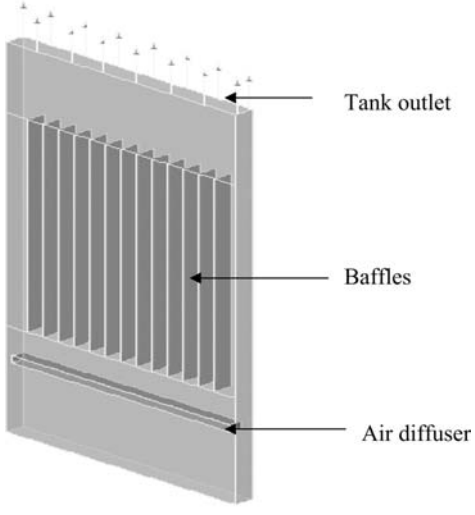

Figure 2. Schematic diagram of the tank showing baffles located between the membrane and the wall.

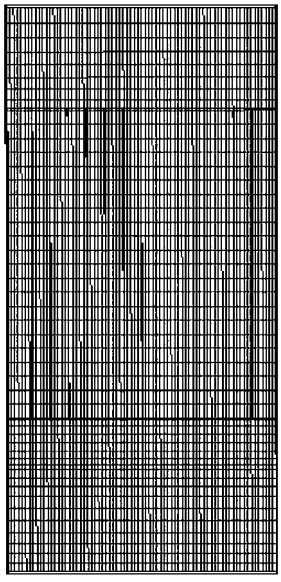

Figure 3. The computational mesh.

condition was set to free slip for air and no slip for water. The top wall of the column was specified as a degassing boundary condition to allow the air to escape. The air diffuser through which gas entered was treated as a volume source of air, having an air flow rate of between 2 and 8 l/min, depending on the experimental condition being modeled.

A constant time step of 5×10^{-2} s was used throughout the simulations. The maximum number of coefficient iteration loops per time step was set to five and this was sufficient to achieve convergence of the residuals during each time step. The high resolution differencing scheme was used with the first order backward Euler scheme being used for the transient terms. The simulations were run for a total real time of 140 seconds. This allowed sufficient time for air to rise to the top of the tank and for the flow to reach a quasi-steady state. Each simulation took about 48 hours on a 2.4 GHz Zeon Intel dual processor.

RESULTS

Two-Phase Flow Characterization

Effect of Nozzle Parameters on Bubble Characteristics

For nozzle sizes of 0.5, 1.0, 1.5 and 2.0 mm, pictures were taken for air flow rates of 2, 4, 6, and 8 l/min or from 20 to 80 $l \cdot min^{-1} \cdot m^{-2}$ of membrane area.

It was found that this range covers typical air flow rates which are used in membrane bioreactors for bubbling in submerged flat sheet membranes which range from 20 to $65 l \cdot min^{-1} \cdot m^{-2}$ of membrane area (19). Some pictures taken for the 0.5 mm nozzle at different air flow rates are shown in Fig. 4. The pictures show an increasing bubble population density as the air flow rate increases. This is expected because an increase in the amount of gas injected should result in an increase in the number of bubbles. A closer

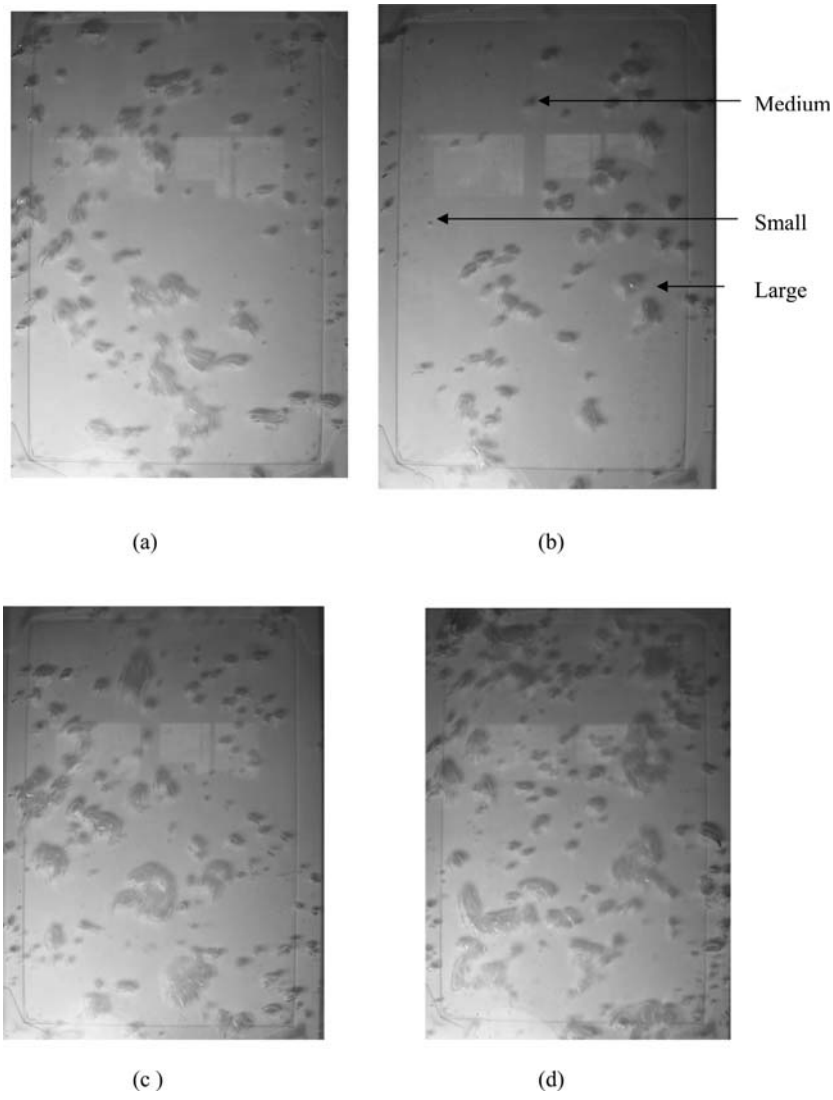

Figure 4. Pictures of two-phase flow at different air flow rates of (a) 2 l/min, (b) 4 l/min, (c) 6 l/min and (d) 8 l/min.

inspection at the pictures shows that the bubbles can be grouped into three categories. There are small (less than 2 mm), medium sized (2–10 mm) and large (greater than 10 mm) bubbles. The large bubbles appear to be more predominant when the air flow rate is increased. The still pictures show that bubbles are well distributed over the membrane surface. What they do not show is that the bubbles towards the center of the column are flowing up whilst those near the edges are flowing down or held almost stationary due to the re-circulation of the fluid in that region.

After the pictures were analyzed with the particle imaging software, for each bubble in each picture a large amount of information was obtained. For the purposes of this study, three parameters were investigated to evaluate their importance to flux enhancement: the bubble area; the bubble mean diameter; and, the total number of bubbles per picture. For each condition, four pictures were analysed and the results combined in order to obtain an average. The total number of bubbles produced at each flow rate for each nozzle is shown in Fig. 5, while Fig. 6 shows the average mean bubble diameter and Fig. 7 shows the average bubble area at each flow rate and nozzle size. Table 1 indicates how many of the small, medium, and large bubbles were present under each condition. The results were also analyzed to obtain the average mean, median, and mode bubble diameter as shown in Table 2. The average mean diameter is calculated by adding the mean diameters for all the bubbles per picture and dividing by the total number of bubbles. The median represents the bubble diameter for which 50% of the bubble population has a mean diameter greater than that diameter and the mode represents the mean bubble diameter with the highest frequency under each condition.

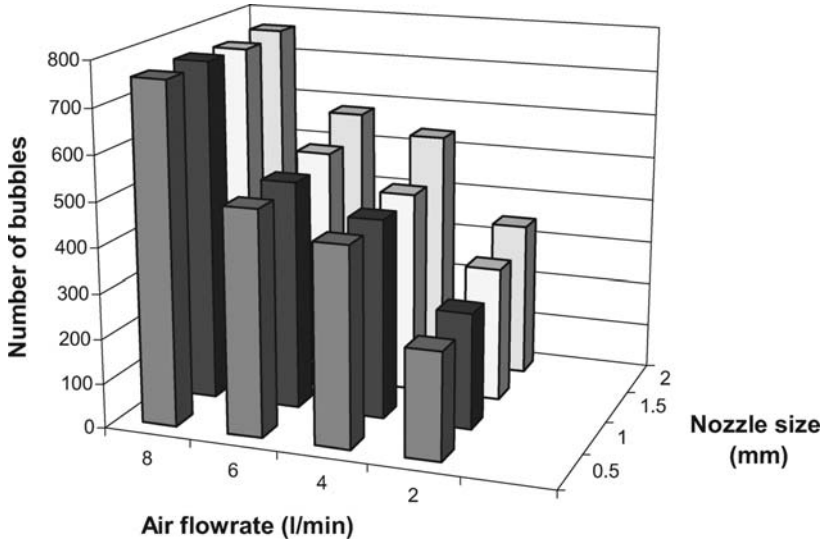

Figure 5. Total number of bubbles per picture for each set of conditions.

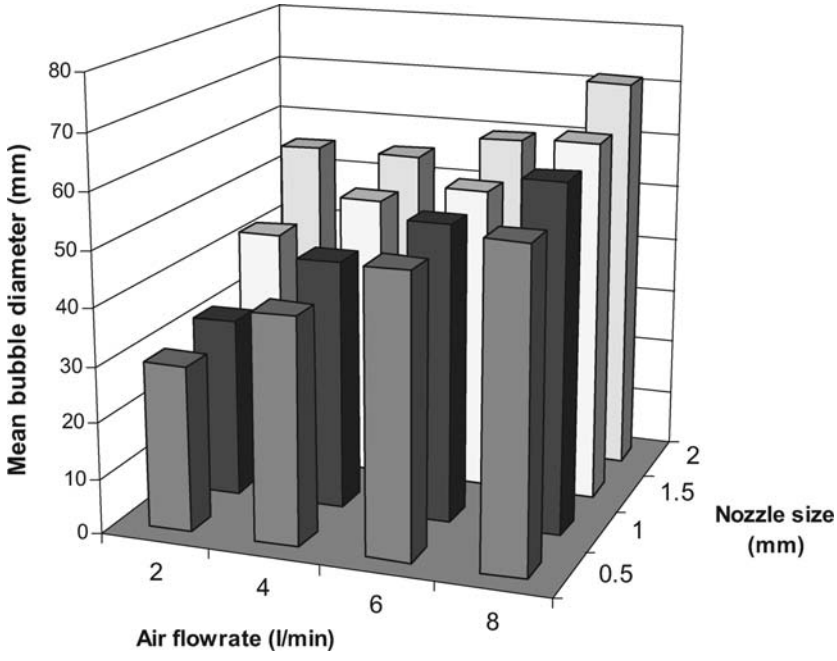

Figure 6. Variation of bubble mean diameter with nozzle size and air flow rate.

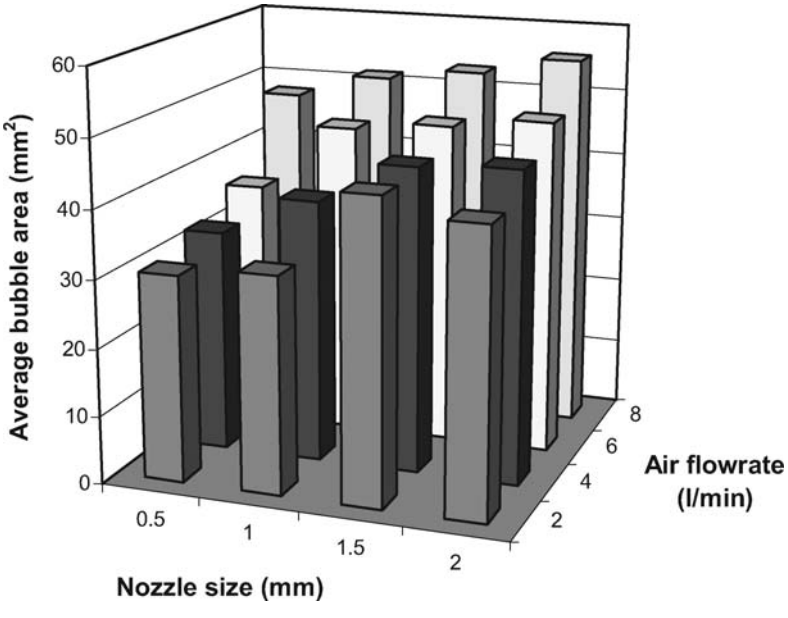

Figure 7. Variation of the bubble average area with nozzle size and air flow rate.

Table 1. Classification of bubbles under different categories

Nozzle size (mm)	Bubble category[a]	Number of bubbles in each category			
		2 l/min	4 l/min	6 l/min	8 l/min
0.5	Small	14	26	29	57
	Medium	102	262	339	546
	Large	61	155	192	223
1.0	Small	11	15	52	72
	Medium	137	290	431	479
	Large	108	201	206	230
1.5	Small	18	36	51	57
	Medium	198	348	375	437
	Large	84	170	211	264
2.0	Small	21	39	47	78
	Medium	204	346	371	554
	Large	128	113	208	218

[a]Small < 2 mm, medium 2–10 mm, large > 10 mm.

From Fig. 5 and Table 1 it can be seen that the number of bubbles and the mean bubble diameter increases with the air flow rate, as does the average bubble area in Fig. 7. On the other hand, the total number of bubbles does not seem to be a strong function of the nozzle size. Table 1 shows that the number of bubbles in each category increases as the air flow rate increases. There are also more bubbles in the medium category than in the other categories for all nozzle sizes and all flow rates. The number of bubbles in the

Table 2. Analysis for mean, median, and mode bubble diameter

Nozzle size (mm)	Bubble diameter (mm)	2 l/min	4 l/min	6 l/min	8 l/min
0.5	Mean	6.96	7.3	8.21	8.87
	Median	7.73	6.17	6.6	6.78
	Mode	2.44	2.5	2.64	2.88
1.0	Mean	7.14	8.63	9.47	9.67
	Median	8.07	8.31	6.01	8.76
	Mode	1.88	2.08	2.18	2.4
1.5	Mean	7.9	8.97	9.51	9.77
	Median	5.31	6.67	5.88	6.36
	Mode	2.02	2.54	2.66	2.74
2.0	Mean	8.22	9.43	9.74	9.92
	Median	5.07	5.21	5.55	5.74
	Mode	2.07	2.15	2.31	2.43

large category is much greater than those in the small category and there are also more large bubbles for the larger nozzles than the smaller nozzles. From Table 2, the median diameter does not show any dependence on the air flow rate or the nozzle size. The mode, which represents the bubble size with the highest frequency, seems to increase slightly with the air flow rate but does not show any trend with regards to the nozzle size, whilst the mean bubble diameter increases with the air flow rate and the nozzle size.

Having classified bubbles in the pictures as either small, medium, or large, we took a step further and calculated what percentage of the incoming air flow ends up as small, medium or large bubbles. This was achieved by calculating the total volume (V) of gas in each of the three categories using data from particle imaging software and then calculating the average rise velocity of bubbles in each category (U). The method used to determine the bubble rise velocities is discussed below. Knowing the height of the tank (H), the residence time (θ) of the gas volume in each category was calculated as H/U. Therefore the volumetric flow rate of the gas in each category was then calculated as V/θ and then this was expressed as percentage of the total gas flow. These data are presented in Fig. 8 which shows that the percentage of flow that ends up as small bubbles is very small, being less than 1% of the total air flow for all nozzles except for the 0.5 mm nozzle where it went up to 1.6%. This figure also clearly shows that most of the air ends up as bubbles with a diameter greater than 10 mm. The percentage of flow in the medium category

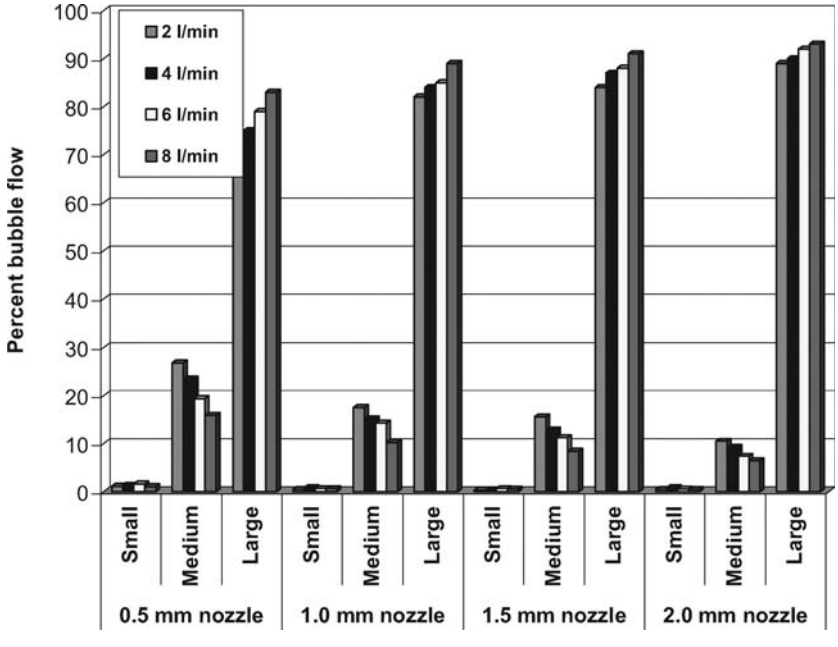

Figure 8. Distribution of flow into small, medium and large categories.

decreases with both nozzle size and air flow rate whilst the percentage of flow as large bubbles increases with both.

Effect of Nozzle Parameters on Bubble Size Distribution

In this section, the effect of air flow rate on the bubble size distribution is analysed in detail. For the purpose of plotting the graphs, because the bubble mean diameter and area varied from very small to very large, bubbles were grouped in categories and the total number of bubbles was calculated in each category for either bubble mean diameter or bubble area. Since there are more bubbles less than 5 mm than any other category, bubbles under 5 mm in diameter were grouped under 0–2 and 2–5 mm categories. Bubbles greater than 5 mm were then grouped in categories of 5 mm difference, for example, 5–10, 10–15, 15–20, up until the bubble size of 70 mm. There were no bubbles found that were larger than 70 mm. The bubble size distribution for the different air flow rates are shown in Figs. 9–12.

From Figures 9 to 12 it is clear that the higher the air flow rate, the greater the number of bubbles in almost all categories of bubble size. In the category of very large bubbles, the smaller air flow rates do not have a single bubble present although one or two large bubbles may appear from time to time. The exception is the larger nozzle of 2.0 mm which produces very large bubbles continuously even at very low gas flow rates. The production of these large bubbles could be the reason why the 2.0 mm nozzle was found to be the most effective at reducing fouling in the experiments (15).

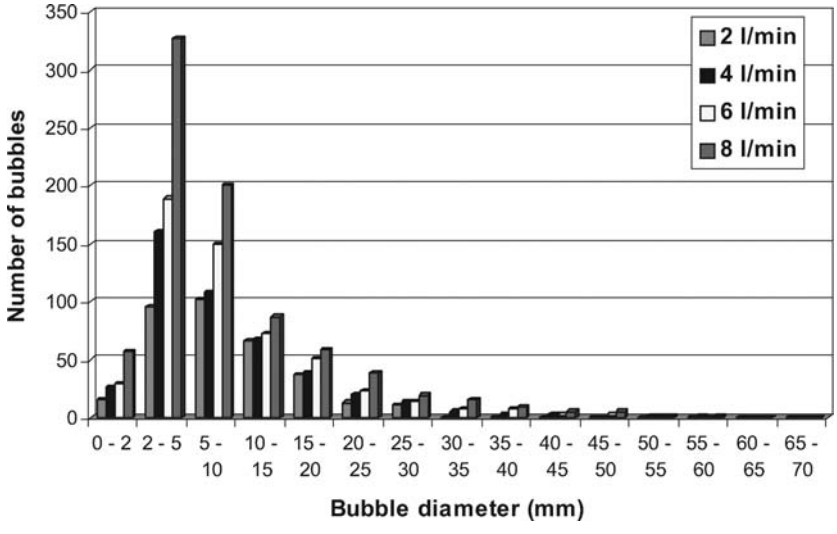

Figure 9. Bubble size distribution for the 0.5 mm nozzle.

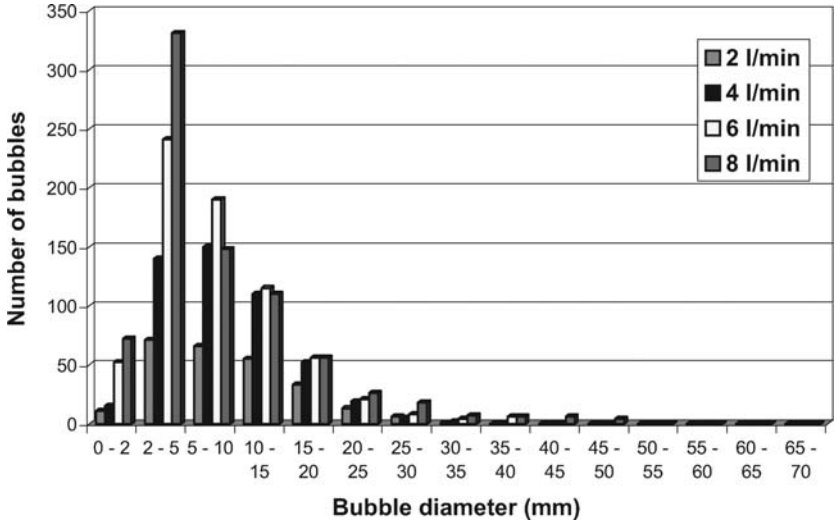

Figure 10. Bubble size distribution for the 1.0 mm nozzle.

Effect of Baffles on Bubble Distribution over the Membrane Surface

As explained in our previous paper (15), one of the reasons for inserting baffles between the membrane and the wall was the observed maldistribution of bubbles over the membrane surface with most bubbles migrating and rising

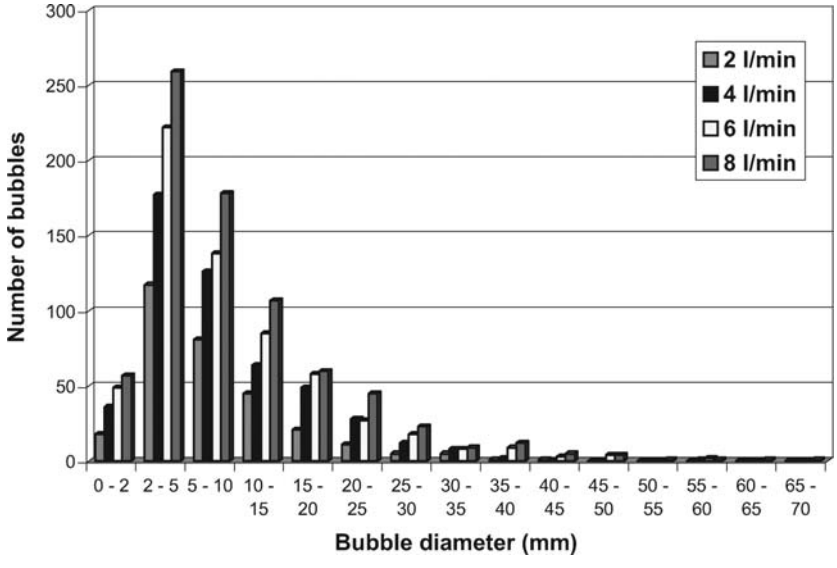

Figure 11. Bubble size distribution for the 1.5 mm nozzle.

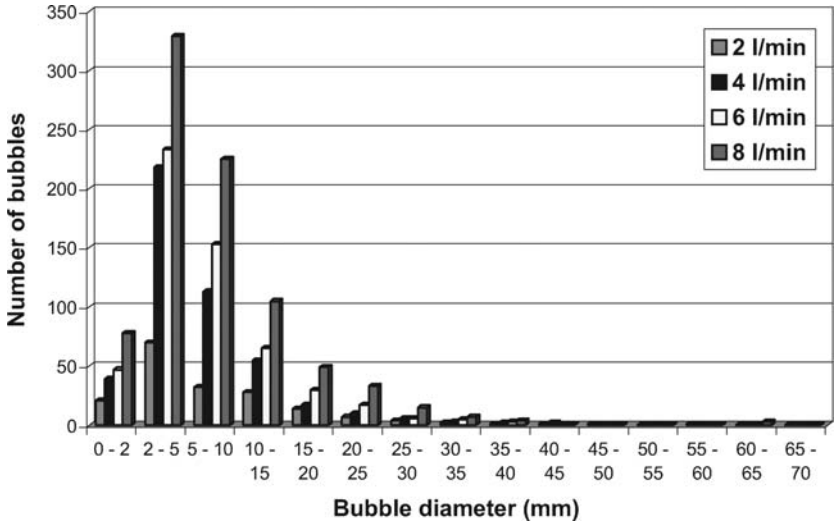

Figure 12. Bubble size distribution for a 2.0 mm nozzle.

towards the centre of the membrane in the absence of baffles. In order to determine to what extent baffles improved the distribution of bubbles, an analysis was undertaken using particle imaging software during which the membrane areas covered by the bubbles (scoured areas) and the areas not covered (unscoured areas) were calculated for both baffled and non-baffled cases. These data are shown in Fig. 13. It can be seen from this figure that the percent scoured area is always higher in cases with baffles than those without at all air flow rates. This figure also reveals that the benefit obtained by using baffles diminishes with the air flow rate. For example, at 2 l/min, the scoured area increases from 17% (non-baffled case) to 32% when baffles are inserted and yet at 8 l/min the increase is from 72% (non-baffled case) to 78% when baffles are present. This could provide a possible explanation for the findings in the previous paper, where it was observed that the differences in the final TMP decrease with the air flow rate when baffles are present.

Determination of the Bubble Rise Velocity

The rise velocity of a bubble in a stationary liquid depends on its size (20). Larger bubbles experience less drag force (per unit volume) than smaller bubbles and will thus rise faster than smaller bubbles. As already noted, bubbles of different sizes were present and vary in diameter from very small (1–2 mm) to very large (40–70 mm). All these bubbles tend to rise at different terminal velocities. In some parts of the column, the rise velocity of the bubbles may have been slowed or accelerated by the re-circulating

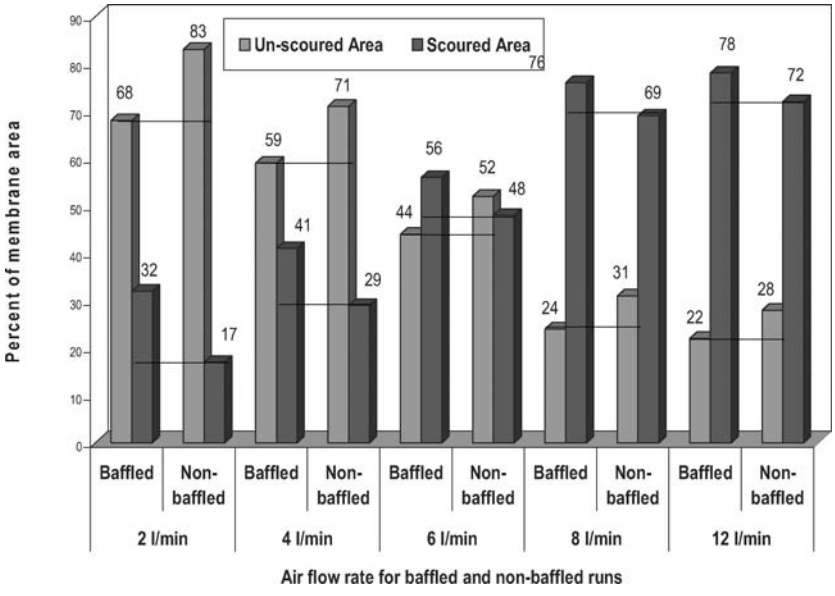

Figure 13. Comparison of scoured and un-scoured areas in baffled and non-baffled cases.

liquid. Therefore, in order to study the effect of air flow rate and nozzle size on the bubble velocity, only the bubbles having almost the same diameter were chosen and only bubbles rising in the central part of the column were considered. This is because towards the center of the column, there appeared to be less downward flow of liquid between the two flat plates. The bulk of the down flow of fluid seems to be towards the edges of the column. The bubbles which were considered for analysis of rise velocity were about 5 mm in diameter and were typically very close to spherical in shape.

The bubble rise velocity was determined using a combination of two software packages, Adobe Premiere 5 and Corel Draw 12. Movies of about 40 seconds duration were recorded using the digital camera. Using Adobe Premiere, the movies were broken down into frames which were 0.04 seconds apart. The exact position of the bubble and the diameter of the bubble in the first frame were determined using Corel Draw. The position of the bubble in the second frame and subsequent frames was also determined in a similar manner. Knowing the time interval between the frames and the distance the bubble had moved during this interval, enabled calculation of the bubble rise velocity. The measurements given by Corel Draw needed to be converted into real time measurements. This was achieved by measuring a distance between two points on the membrane, taking a photograph of the membrane and then using Corel Draw to measure the same distance. The camera settings were the same as those used to record the movies so that the magnification of the images was the same. The ratio obtained from

these two measurements was then used to convert all the Corel Draw measurements into real time measurements.

Figure 14 shows the effect of air flow rate on the bubble velocity. For the 5 mm bubbles analyzed in this study, the bubble rise velocity increased with the air flow rate. For example, for the 2 mm nozzle, the bubble rise velocity was 460 mm/s when the air flow rate was 2 l/min and the rise velocity was 710 mm/s when the air flow rate was 8 l/min. Thus for a fourfold increase in air flow rate, the bubble rise velocity increased by almost 36%. Figure 14 also reveals that the bubble rise velocity increased with the nozzle size for all air flow rates examined, with the 2.0 mm nozzle producing the highest bubble velocity and 0.5 mm the lowest. This is contrary to what has been found in some studies in which the bubble rise velocity decreased with the nozzle size (21). Le-Clech et al. (22) obtain the same rise velocity for nozzles of different sizes. This discrepancy could be due to the fact that these other studies were looking at an individual bubble instead of one bubble rising in a cluster of bubbles, as in this study.

If the column is long enough, bubbles of the same size should theoretically reach the same terminal rise velocity. The terminal velocity of air bubbles with a diameter of 5 mm rising in water, can be predicted from the following equation (1) developed by Beek and Muttzall (23), which predicts a terminal velocity of about 0.24 m/s for a 5 mm bubble. This velocity is almost 40% lower than the smallest velocity that was measured in this study. The discrepancy could be due to the fact that equation (1) was developed for single bubbles rising in stationary liquids. In our case there are swarms of bubbles rising, inducing a large amount liquid recirculation. The re-circulating liquid seems to have increased individual bubble velocities

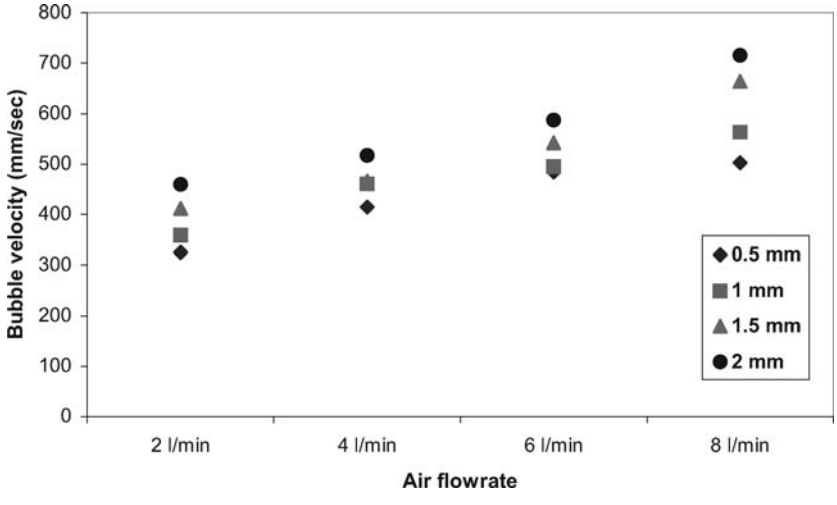

Figure 14. Calculated bubble rise velocities for a bubble of about 5 mm diameter.

in the center of the column. The larger the bubble, the larger the amount of liquid recirculation induced and hence the observed effect of increased velocity with air flow rate and nozzle size.

$$U_b = \sqrt{\frac{2\sigma}{\rho d_b} + \frac{(\rho - \rho_b)}{\rho}\frac{g d_b}{2}} \quad (1)$$

where, U_b is the terminal bubble rise velocity, σ, is the surface tension, ρ, is the density, g is gravitational acceleration, and d_b is the diameter of the bubble.

CFD Simulations

Firstly, the effect of inlet air flow rate on gas and liquid flow profiles is presented, followed by the effect of bubble size. Then the membrane wall shear stress distribution is discussed and lastly the effect of the baffles on the wall shear stress at the membrane surface is presented. The predicted influence of gas velocity, bubble size, and baffles on flow profiles and wall shear stress are compared with experimental data in the discussion section.

The influence of Gas Inlet Velocity

In this section the effect of the air injection rate on the gas and liquid velocity flow profiles in the tank is examined. The bubble diameter for these simulations was specified as 5 mm. Figure 15 shows the computed vector plots for superficial gas velocity profiles at different times for the flow rate of 8 l/min. A similar flow profile was observed for different air flowrates. Figure 16 shows a comparison between flow profiles when the airflow rates are 2 and 8 l/min at the same time in the simulations (that is, after 140 s of simulations). From Fig. 15 it can be seen that as soon as the gas leaves the diffuser it moves towards the edges of the column as it rises. The gas divides into two main streams that flow upwards near the edges of the column. In addition, these two main plumes of gas move up in a meandering manner. The degree of meandering was small for the low air flow rate of 2 l/min and was much higher at the higher flow rate of 8 l/min. This phenomenon of bubble swarms meandering has been reported by other researchers (24–26). Buwa and Ranade (26) found that the amplitude of the gas plume oscillation increased with an increase in the gas flow rate, with bubbles almost touching the sidewalls at very high gas flow rates. According to Delnioj et al. (27) it is the vortices in the liquid stream that causes the gas to move in a meandering fashion. At low gas flow rates, Kuwagi et al. (28), observed that the gas bubbles rise almost in a straight line in a stagnant liquid and start to move in a zigzag fashion only when the gas flow rate is increased.

The flow pattern described above differs somewhat from what was observed experimentally at air flow rates of 4 l/min upwards. In the

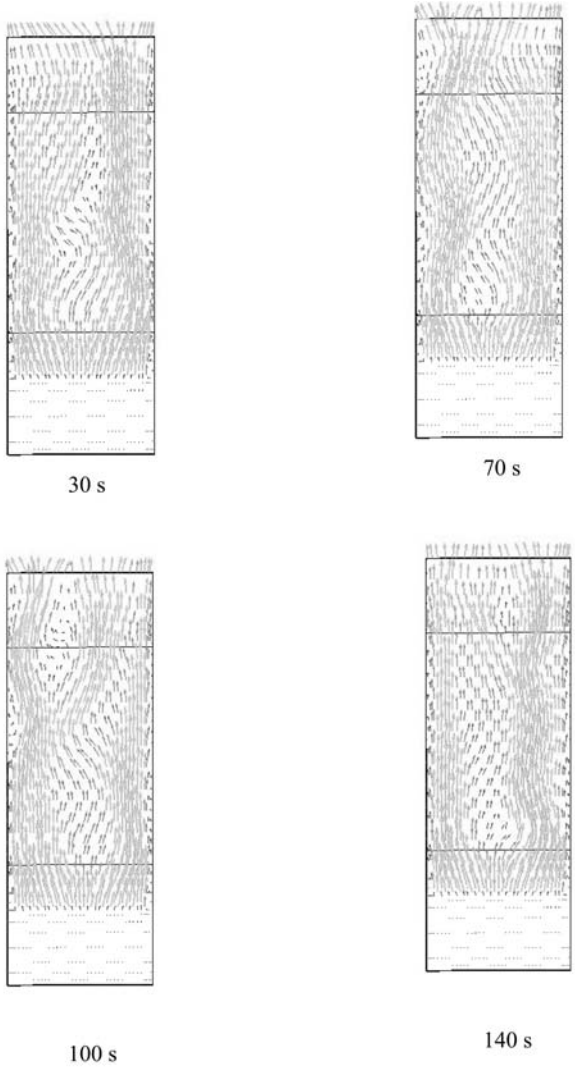

Figure 15. Air superficial velocity profiles at different times for an air flow rate of 8 l/min. The maximum air velocity is about 0.36 m/s.

experiments, bubbles were observed moving away from the column edges towards the centre except for the lower flow rate, such as 2 l/min, where bubbles rose in an almost rectilinear path. The migration of bubbles towards the column center has also been observed on other bubble column studies (29, 30). It is not clear what constituted this difference in the observed and simulated flow patterns but it may be linked to the fact that it was difficult to model the gas sparger exactly as it was in the experiments.

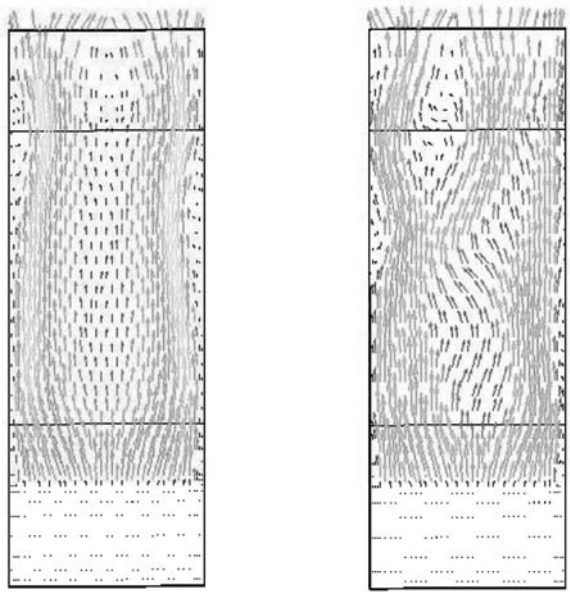

Figure 16. Air superficial velocity profiles after 140 s of simulations for air flow rate of (a) 2 l/min and (b) 8 l/min. The maximum air velocity is about 0.36 m/s.

Effect of Bubble Size on Air and Water Velocity Profiles

Recently Buwa and Ranade (31) have reported experimental data on the dynamics of gas-liquid flows with different spargers, as well as with different gas injection rates. Their results indicated that the key dynamic characteristics depend on the bubble size and bubble size distribution. However, with the current two-fluid model we were only able to study the effects of bubble size and unable to account for size distribution. One of the limitations of the standard Eulerian two-fluid model available is that the bubble size has to be specified and only one bubble size can be used per simulation. All the results presented in the previous section were obtained with a bubble size of 5 mm. In the actual experiments, a bubble size distribution exists at all air flow rates as revealed in section "Effect of Nozzle Parameters on Bubble Size Distribution". The analysis done in section "Effect of Nozzle Parameters on Bubble Size Distribution" indicated that the bubble size does play a role in terms of the effectiveness of two-phase flow on membrane cleaning. In order to obtain some further understanding of the effect of bubble size per se on the efficiency of the two-phase flow, simulations were made with different bubble sizes and the results were compared. For these investigations the air flow rate was kept constant at 4 l/min. This air flow

rate was chosen because, based on the previous results, at this air flow rate, the meandering of the gas is just starting to become pronounced, whereas at 2 l/min bubbles rise almost vertically.

Figure 17 presents water superficial velocity profiles for bubbles of different sizes at the end of the simulation. These vector plots show an increase in the degree of meandering as the bubble size is increased. For the

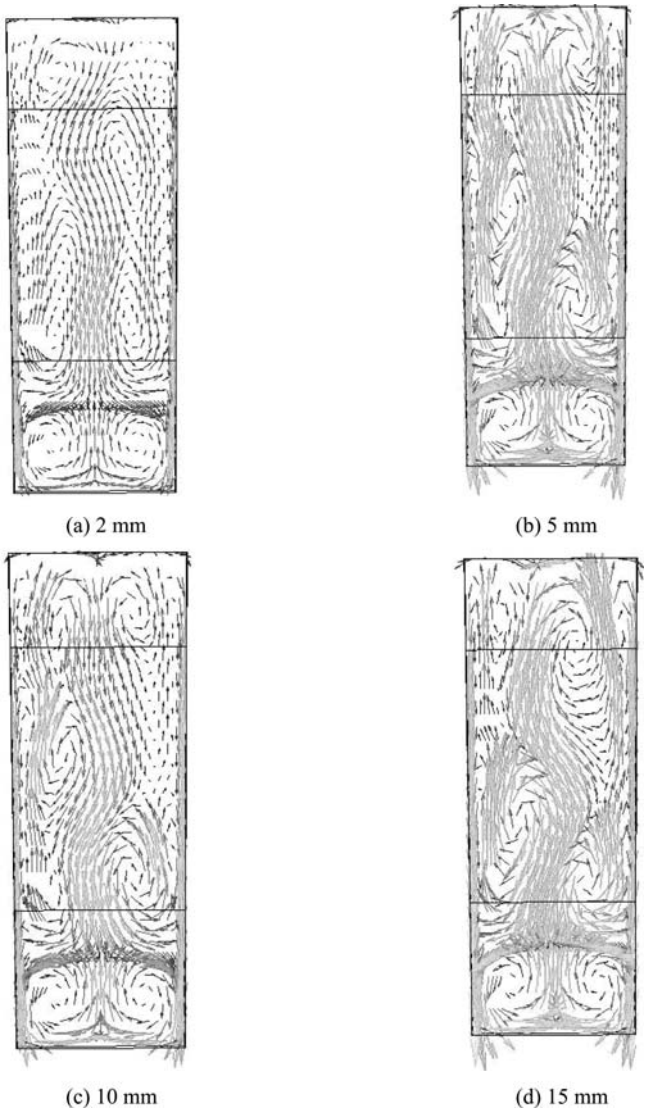

Figure 17. Water superficial velocity profiles for bubbles of different sizes at the end of the simulation. The water velocity ranges from 0.36 to 0.58 m/s.

2 mm bubbles (Fig. 17a), there is a slight sideways movement of the water stream but when the bubble size is 15 mm (Fig. 17d) the amplitude of the water stream meandering is increased quite significantly. Similar observations were made by Buwa and Ranade (26), who noted that the plume oscillation period of around 10 s for larger bubbles (20 mm) was much greater than that of smaller bubbles (5 mm). The improved liquid recirculation at larger bubble sizes may assist in minimising fouling on the membrane. The 15 mm bubbles used in the simulations are not as large as some of the bubbles that were measured experimentally which were about 70 mm but the bubble size distributions reported in section "Effect of Nozzle Parameters on Bubble Size Distribution" indicated that the percentage occurrence of such large bubbles is low and that the bubble size with the highest frequency was 4 to 5 mm. Thus the simulation results obtained using a 5 mm bubble can be used with confidence in terms of understanding the overall behaviour of the experimental system. The effect of bubble size on membrane shear stress is discussed in the following section.

Analysis of Shear Stress Distribution on the Membrane Surface

It is generally accepted in the literature that flux enhancement by two-phase flow is partly due to enhanced shear stress on the membrane (32–34). Cabassud et al. (33) have been able to develop a correlation between shear stress and flux enhancement by measuring shear stress using an electrochemical method. The main objective of this study is to analyze the shear stress distribution on the membrane surface through CFD and to determine how it varies with changes in the experimental conditions, such as an increase in air flow rate, an increase in bubble size, and how it is affected by the use of baffles. Figure 18 shows the shear stress distribution on the membrane surface at the end of the simulations for different air flow rates. To make the comparison easy, the maximum shear stress shown on each plot has been limited to 0.5 Pa. All the pictures in this figure show that regions of high shear stress coincide with the regions where there is strong upflow of air, for example near the column edges. In the centre of the column, where there is mostly water flowing down, the shear stress is relatively low despite the fact that maximum downward velocity of water is almost the same as that of the upward velocity. Therefore, the regions of high shear stress coincide with the presence of bubbles. This phenomenon has been observed experimentally in cross-flow tubular filtration (35), where the shear stress was higher in the presence of bubbles than when liquid was flowing alone, even though the superficial liquid velocity was similar in both cases.

From Fig. 18 it can also be seen that the average area of high shear stress increases with the air flow rate. Thus, at higher liquid flow rates there are more areas of the membrane which are exposed to a high shear stress. With less meandering of air, as in low air flow rates, the area of the membrane which does not experience high shear also increases. Therefore, it can be

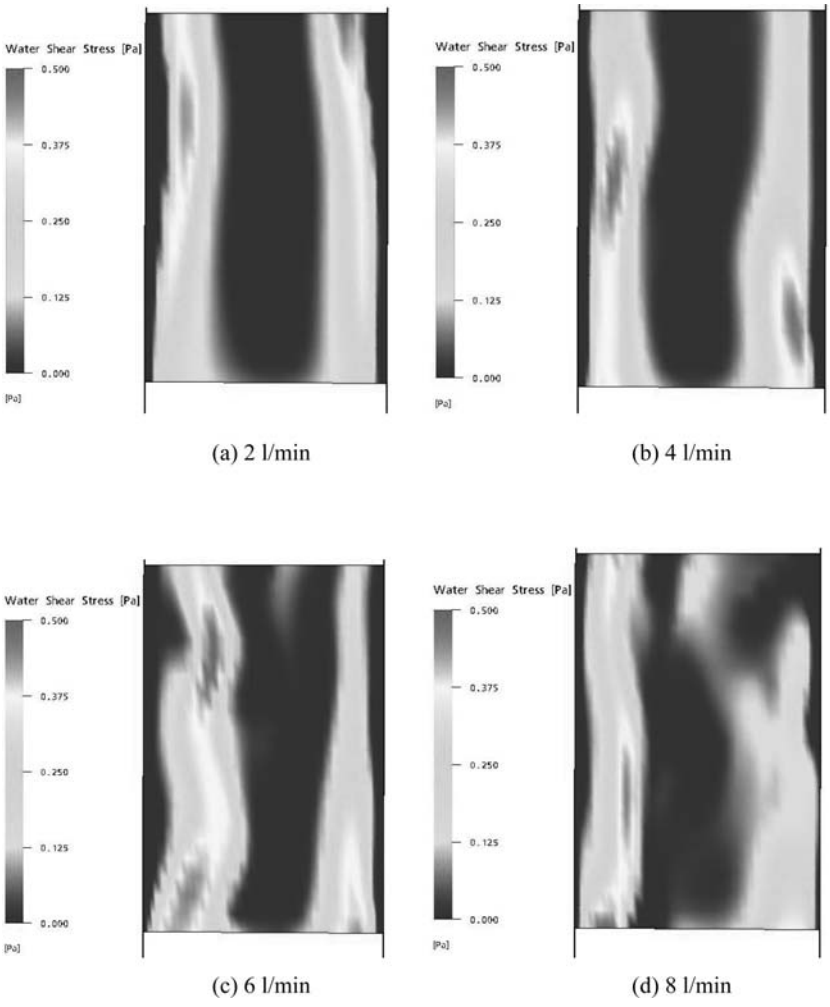

Figure 18. Shear stress distribution at the end of the simulation for different air flow rates.

concluded that a better distribution of air across the membrane will lead to a better distribution of shear stress and thus enhance the efficiency of the gas-liquid two-phase flow cleaning process. This can be achieved by using baffles and is examined in "Effect of Baffles on the Efficiency of Two-Phase Flow Flux Enhancement".

The effect of bubble size on the membrane shear stress has also been examined. Figure 19 shows the shear stress distribution on the membrane at the end of each simulation for different bubble sizes. To make comparison of the plots easy, the maximum shear stress shown in each picture is again limited to 0.5 Pa. From these pictures it can be observed that higher shear

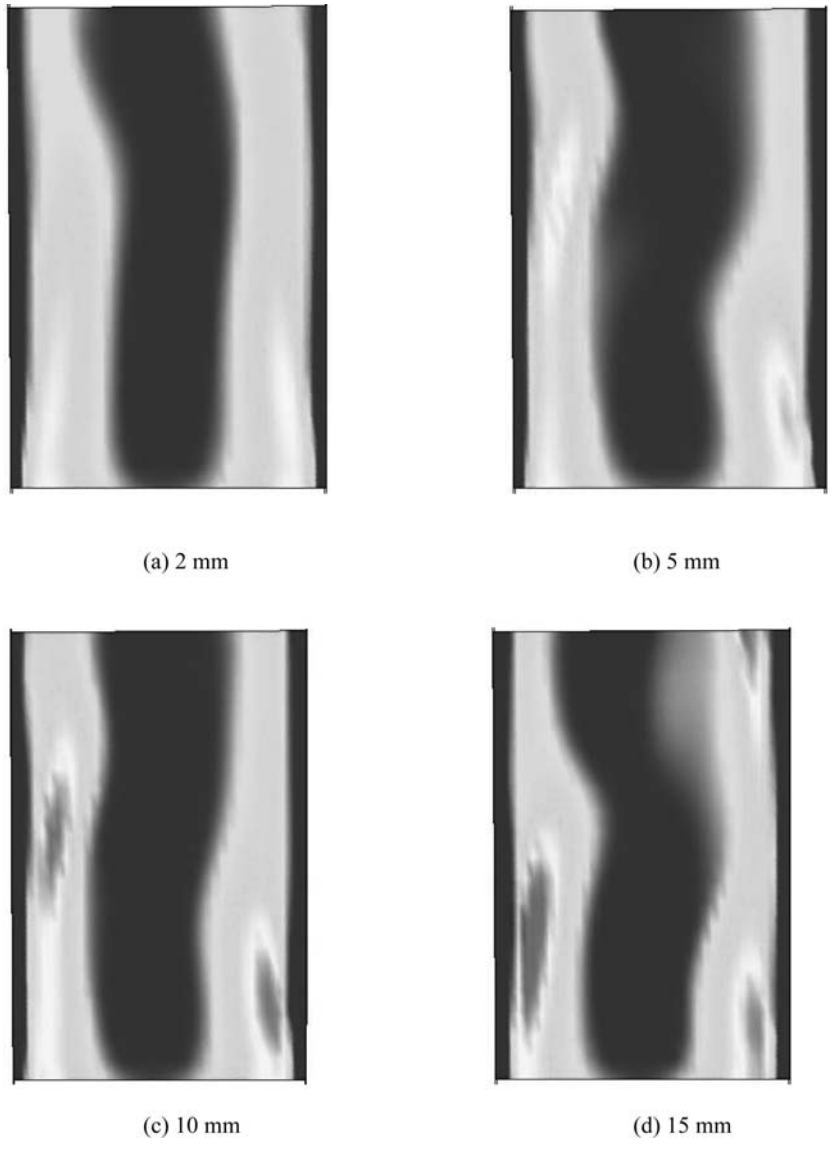

Figure 19. Shear stress distribution at the end of the simulation for different bubble sizes.

stresses cover a larger area for the larger bubble sizes of 10 and 15 mm. The maximum shear stress for the 2 mm bubbles, for example, is below the specified maximum of 0.5 Pa. The conclusion is therefore that the shear stress increases with the bubble size and that the distribution of shear stress across the membrane also improves with bubble size.

The average shear stresses and the maximum shear stresses on the membrane were calculated at ten seconds intervals from the start to the end of the simulation at different air injection rates and different bubble sizes. The average shear stresses were always found to be highest for the air flow rate of 8 l/min and lowest for 2 l/min at any time during the simulations even though the average shear stresses were fluctuating from time to time (Fig. 20). On the other hand, the maximum shear stress was found to be constant for most of the time during the simulation. The maximum value of the shear stress was found to increase with the air flow rate (Fig. 21). From 2 l/min to 8 l/min the maximum shear stress increased from 0.491 Pa to 0.711 Pa which represents an increase of about 31%. Therefore it can be concluded that the greater meandering of the gas stream seen at higher air flow rate is accompanied by an increase in the overall imposed shear stress on the membrane which would be good for the membrane cleaning process. However, a balance needs to be maintained between high shear rates from high air flow rates and energy consumption. The maximum shear stress also showed an increase with the bubble size up to a bubble size of 10 mm (Fig. 22). When the bubble size was increased from 10 to 15 mm, the increase in maximum shear stress was minor.

Effect of Baffles on the Efficiency of Two-Phase Flow Flux Enhancement

For submerged flat sheet membranes, there exists a small gap between the membrane plates. The size of this gap varies from one commercial system

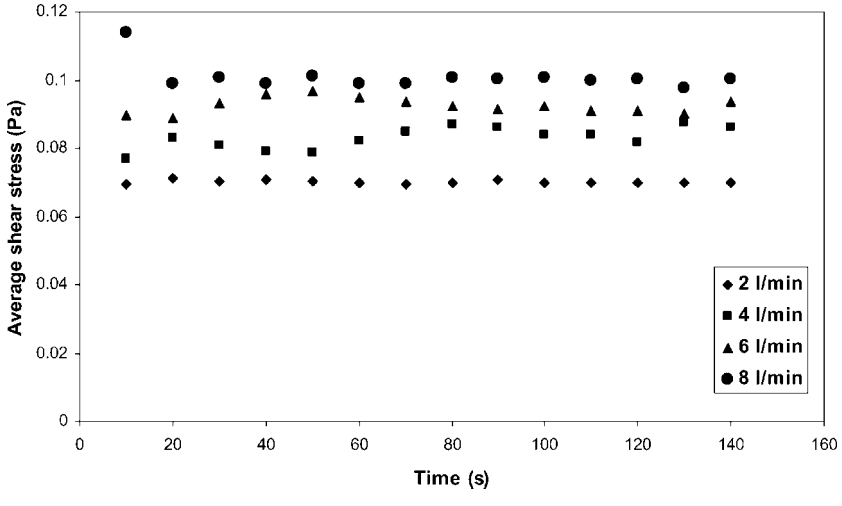

Figure 20. The evolution of average shear stress with time at various air flow rates.

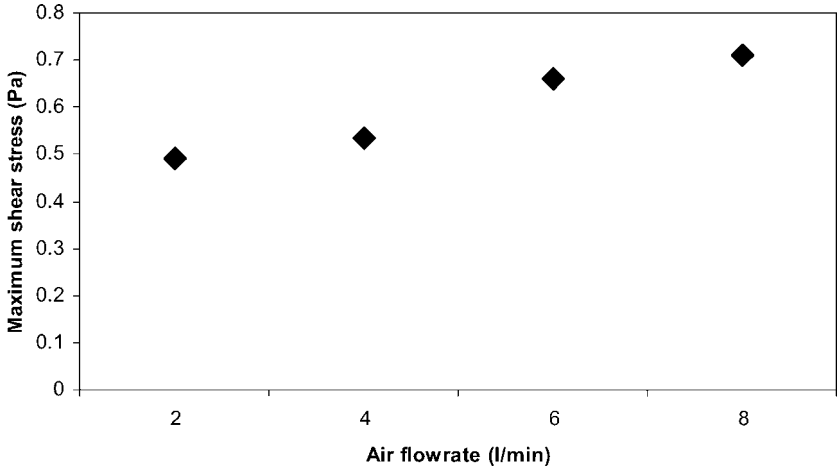

Figure 21. Maximum shear stress on the membrane versus air flow rate.

to another. Since in this study only one flat sheet membrane was involved, the gap between the membrane and the wall was kept fixed at 7 mm, which is a typical gap used for the Kubota membrane bioreactor process (36). Visual observations from the experiment show that the bulk of the air when flowing across the membrane migrates towards the center of the column despite the fact that the air inlet nozzles are distributed evenly across the bottom of the tank. This uneven distribution of air across the

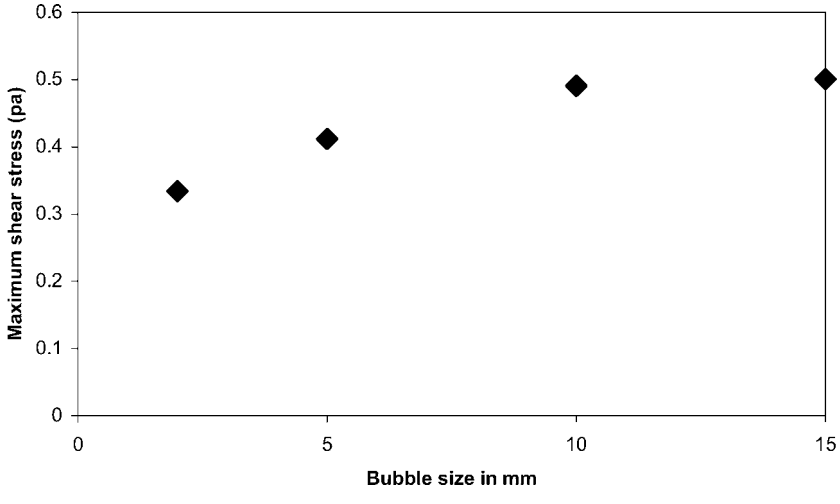

Figure 22. Maximum shear stress on the membrane versus bubble size.

membrane causes some parts of the membrane to be cleaner than others and this situation can be improved by the insertion of baffles between the membrane and the wall in order to attain a better distribution of air. The use of baffles in the experiments improved trans-membrane pressure reduction but the actual reason why baffles are more effective is not yet fully understood. Thus, simulations with baffles inserted in the geometry were conducted in order to obtain a better understanding of why baffles are effective.

In the experiments presented in our previous paper (15) only a fixed number of baffles (13 baffles) were used but in the simulation the number of baffles was varied in order to gain an insight into the effect of the number of baffles as well. Simulations were conducted with 3, 7, and 13 baffles (equally spaced across the membrane) and these results were compared with the case without baffles, which have been presented in the previous sections. For the simulations with baffles, only the bubble size of 5 mm was used and air flow rates of 2 to 8 l/min were investigated, however, the results presented here are only for the air flow rate of 8 l/min, as similar effects or trends were obtained with the other air flow rates. Figure 23 shows air superficial velocity vectors for simulations with different numbers of baffles. Clearly the case with no baffles shows meandering of air which becomes limited as baffles are inserted and the number of baffles is increased. The case with 3 baffles does show a slight meandering of the bubble plume but for 7 and 13 baffles the air is distributed uniformly across the membrane, so that each part of the membrane is exposed to almost the same amount of air flow which implies that overall shearing over the entire membrane surface is almost uniform.

Figure 24 shows shear stress plots on the membrane surface at the end of the simulations for cases with different baffles. For effective comparison of the plots, the maximum shear stress displayed in each plot has been fixed at 0.5 Pa. It is evident that the size of the regions of high shear stress increases as the number of baffles is increased. The area of low shear stress is very large in the case with no baffles covering almost more than half of the membrane, whereas in all the cases with baffles the low shear stress area is very small. The values of the average and maximum shear stress on the membrane were extracted at ten seconds intervals during the simulation to monitor their progression. It was found that both the average and maximum shear stress values did not change significantly with time for the cases with baffles, unlike in the case without baffles, where the average shear stress varied substantially with time during the simulation. Figure 25 shows that the maximum shear stress increases with the number of baffles. From the case without baffles to the case with 13 baffles, the maximum shear stress increased by about 29%. The average shear stress over the entire membrane surface also increased with the number of baffles (Fig. 25). The average shear stress for the case without baffles was computed and is also shown in this figure.

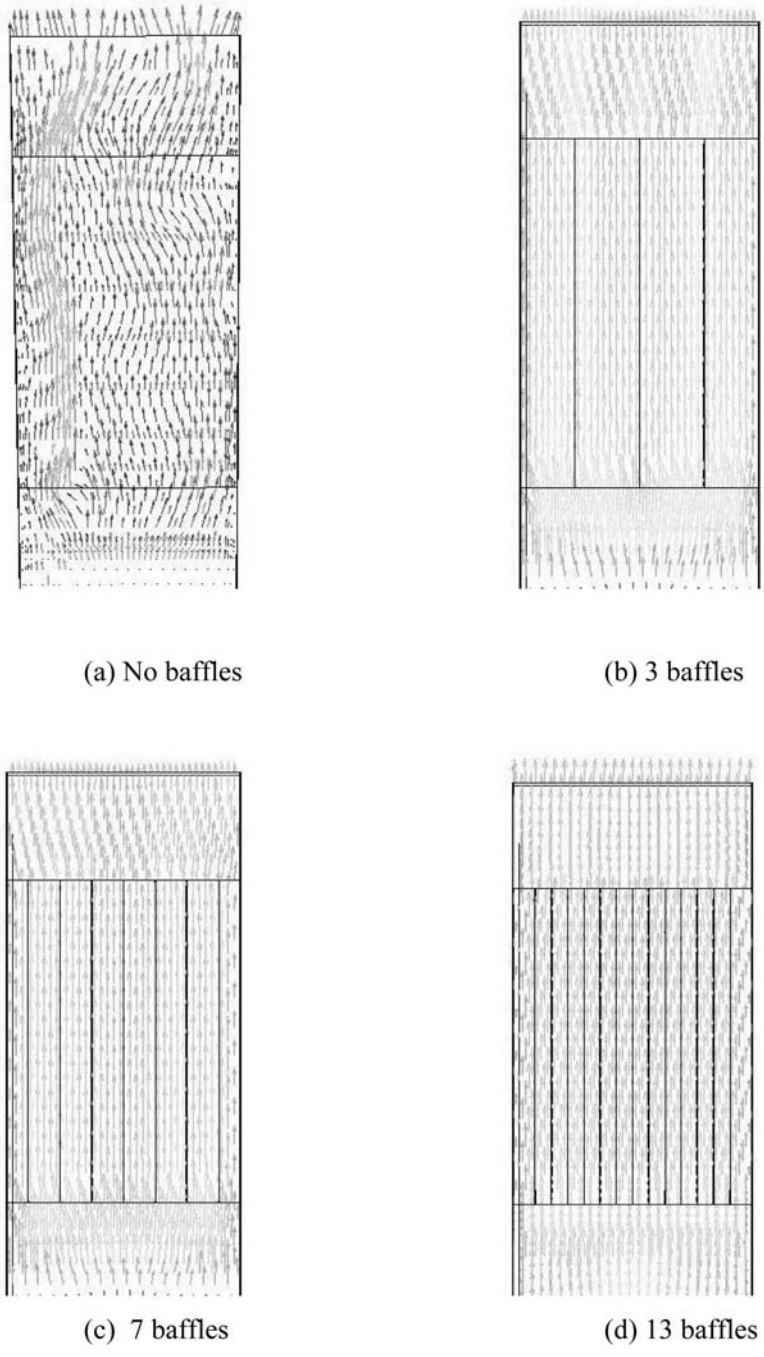

Figure 23. Air superficial velocity profiles for runs with different number of baffles at 8 l/min.

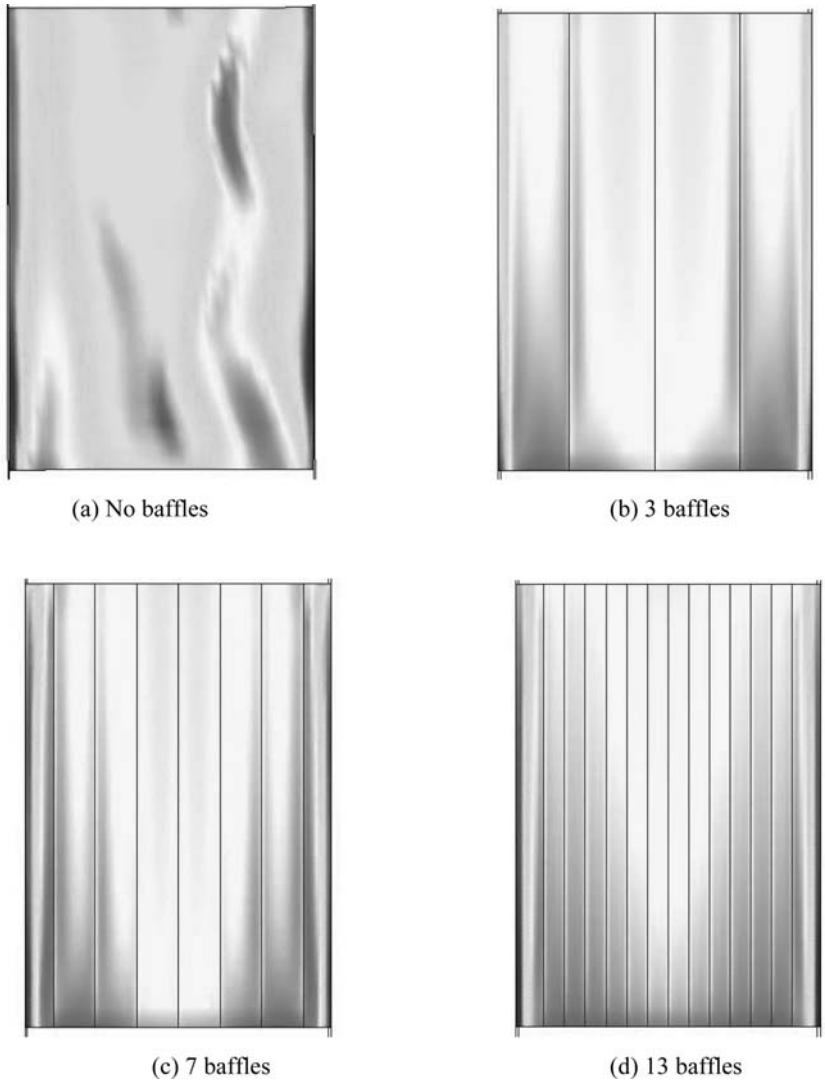

Figure 24. Shear stress distribution on the membrane for simulations with different numbers of baffles at an air flow rate of 8 l/min.

DISCUSSION AND CONCLUSIONS

The use of the particle imaging software AnalySIS® has been helpful in providing information regarding the effectiveness of gas-liquid two-phase flow in reducing fouling rate for submerged flat-sheet membranes. The information obtained in this study has explained some of the trends observed in the experiments presented in our previous paper. In the analysis of the

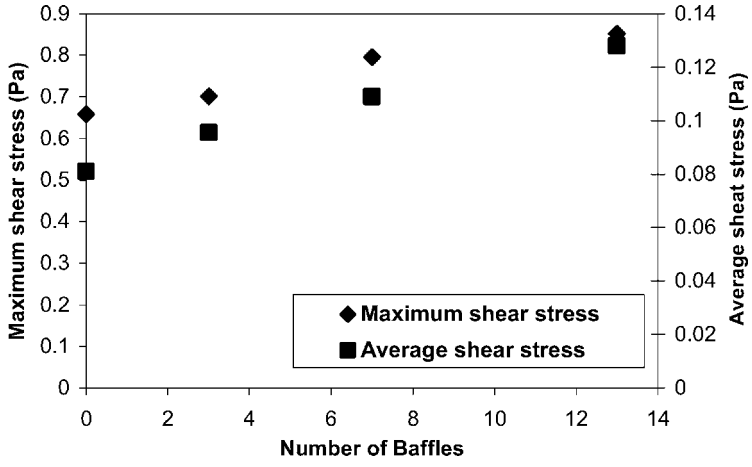

Figure 25. Maximum and average shear stress on the membrane versus number of baffles.

pictures it was observed that the frequency of medium and large bubbles is higher for the higher air flow rates (6 and 8 l/min) and larger nozzles (1.5 and 2.0 mm). However, the number of small bubbles also increased with the gas flow rate and nozzle size. Further analysis into the distribution of flow into small, medium, and large categories revealed that although there were more bubbles in the medium category, the actual amount of air in these bubbles is significantly less than the air contained by bubbles in the large category. Thus looking at the number of bubbles alone does not tell a complete picture. From this analysis it was clear that as the air flow rate and nozzle size increased, the fraction of air in the large flow category also increased. Having determined in the previous paper that the extent of fouling reduction increases with nozzle size and air flow rate, therefore these results suggest that large bubbles play a much more dominant role in combating fouling than small bubbles. The channel gap width between the membrane and the wall was 7 mm. Therefore bubbles greater than 7 mm effectively became slugs or Taylor bubbles. For these types of bubbles there exists a thin falling film between the bubble and the membrane. Shear stresses in this film are known to be very high (13, 14). Also behind the Taylor bubble, the falling film reverses flow direction and this creates a turbulent wake behind the bubble. This could therefore shed some light into the increasing fouling reduction obtained as bubbles became larger and the number of large bubbles increased.

At low gas loading rate, there is relatively little disturbance caused by the bubbles on the liquid phase. The bubbles are seen to rise almost in a straight-line. The bubbles rise smoothly through an almost stagnant liquid without causing much agitation and liquid recirculation. However, as the gas flow

rate is increased, the system becomes more and more unstable. The majority of the bubbles start to migrate to the centre of the column and move vigorously in a zigzag manner. There is strong up-flow of liquid in the centre of the column following the bubbles and strong down-flow near the walls. The down-flow of liquid near the walls is evidenced by bubbles either flowing down or held almost stationary in that vicinity. This flow pattern was also observed by Torvik and Svendsen (37) and by Delnoij et al. (27) in bubble columns almost identical to the one studied here. Thus, with higher gas flow rates, there is a greater mixing or turbulence in the system which helps to explain the improvement in flux.

Data presented in this paper has shown that the area of the membrane scoured by the air bubbles increases when baffles are inserted, showing that better distribution of the bubbles is achieved by using baffles. Also from the previous paper, the presence of baffles was shown to increase fouling retardation for gas-liquid two-phase flow. This increase in the fouling retardation can therefore be linked to the fact that more of the membrane is scoured by air when baffles are presented. Another possible reason why baffles are seen to be more effective could be that when baffles are inserted, small rectangular channels (7 mm × 10 mm) are created through which the air can flow. Bubbles larger than 7 mm in diameter effectively become slugs. Thus with baffles present the most dominant type of two-phase regime in the channel becomes slug flow. Slug flow is known to be the most effective two-phase flow regime for tubular and hollow fiber membranes (12). Thus by analyzing the characteristics of two-phase in submerged membrane channels, it sounds reasonable to conclude that the larger the air bubbles the better the cleaning effect will be. However, for submerged hollow fibers the trends seem to be reversed, that is, smaller bubbles are more effective than larger bubbles (38). For submerged flat sheet membranes, it is possible that an optimum bubble size exists but could not be elucidated experimentally due to the fact that bubble size could not be controlled when bubbles are generated. However, the effect of bubble size and shear stress distribution on the membrane could be assessed via CFD simulations.

The Eulerian two-fluid CFD simulations were carried out mainly to investigate the hydrodynamic features of two-phase flow that are responsible for flux enhancement in the submerged flat-sheet membrane system. Increasing the gas injection rate resulted in greater meandering of the gas and liquid streams in the tank. The amplitude of meandering was also higher with the higher gas flow rate. This implies that with more air, there is greater mixing occurring in the tank. Greater mixing of the liquid will minimize the extent to which particles will settle on the membrane, thus, fouling will be reduced and flux will be enhanced. With the lower air flow rate the meandering is small and restricted only to certain parts of the membrane, whereas at higher air flow rates the meandering is large and spreads over large parts of the membrane. This could

therefore explain why, with the lower gas flow rates, the flux enhancement is lower compared with higher gas flows.

The effect of increasing the bubble size also resulted in an increase in the degree of meandering of the gas and liquid streams just as increasing the air flow rate did. Moreover, increasing the bubble size also had an effect on the maximum induced liquid velocity, with the largest bubble size of 15 mm inducing the largest superficial liquid velocity. This could partly be due to the fact that larger bubbles rise faster. In tubular systems, the shear stress on the membrane has been found to be directly proportional to the liquid velocity across the membrane (33) and thus larger bubbles may be more effective in reducing fouling due to increased induced liquid velocities. In the characterization of two-phase flow, it was observed that the frequency of larger bubbles is much higher at higher air flow rates, which helps to explain why the higher air flow rates were found to be more effective in the experiments.

Wall shear stress is probably the major factor responsible for reduction of fouling in membrane systems. All fouling minimization strategies have focused on improving the shear stress on the membrane by creating turbulence (39). Analysis of the shear stress distribution on the membrane showed that the areas of higher shear stress on the membrane coincide with regions where the bulk of the air passes through. The size of the regions of high shear stress increased as the air flow rate increased. Also the locations of these regions varied with time during the simulation depending on the path of air flow, thus covering a large fraction of the membrane area over time, particularly at higher gas flow rates. The average shear stress on the membrane was always higher at the air flow rate of 8 l/min than the smaller air flow rates at any time during the simulation. The maximum shear stress increased with both the air flow rate and the bubble size. This analysis of the shear stress is helpful in understanding the trends observed experimentally where the degree of fouling reduction increased as the air flow rate was increased.

Baffles were used in the experiments in order to improve the distribution of flow across the membrane. The simulations were thus carried out to help understand how the presence of baffles affects the flow distribution and the shear stress across the membrane. In the simulations the number of baffles was varied to gauge whether the number had any effect. It was observed that the presence of baffles completely stopped the meandering of the gas and liquid stream resulting in the bubbles rising in a straight path. There was no migration of bubbles towards the edges of the column. Analysis of the shear stress on the membrane surface revealed that most of the membrane experienced larger shear stresses when baffles are present as compared with the cases without baffles. Both the average and the maximum shear stress also increased with the number of baffles. In the experiments, fouling control improved when baffles were present at all flow rates. This increase in fouling reduction can therefore be clearly linked with an

increase in overall shear stress on the membrane. The increase of shear stress with the number of baffles shows that as the bubbles become more confined they exert a higher shear stress on the membrane. However, the number of baffles can only be increased to a certain extent, as they obstruct membrane area and could become blocked and increase the pressure drop to unacceptable levels.

ACKNOWLEDGEMENTS

The authors gratefully acknowledge financial support from AusAID in Australia and the NRF in South Africa.

REFERENCES

1. Visvanathan, C., Ben Aim, R., and Parameshwaran, K. (2000) Membrane separation bioreactors for wastewater treatment. *Crit. Rev. in Envronm. Sci. Technol.*, 30: 1–42.
2. Chiemchaisri, C., Yamamoto, K., and Vigneswaran, S. (1993) Household membrane bioreactor in dometic wastewater treatment. *Water. Sci. Technol.*, 27 (1): 171–178.
3. Fakhru'l-Razi (1994) Ultrafiltration membrane separation for anaerobic wastewater treatment. *Water Sci. Technol.*, 30 (12): 321–327.
4. Côté, P. and Buisson, H. (1997) Immersed membrane activated sludge for the reuse of municipal wastewater. *Desalination*, 113 (2–3): 189–196.
5. Stephenson, T., Judd, S., Jefferson, B., and Brindle, K. (2000) *Membrane Bioreactors for Wastewater Treatment*. IWA Publishing: London.
6. Lee, C.K., Chang, W.G., and Ju, Y.H. (1993) Air slugs entrapped cross-flow filtration of bacterial suspensions. *Biotech. and Bioeng.*, 41: 525–533.
7. Bellara, S.R., Cui, Z.F., and Pepper, D.S. (1996) Gas sparging to enhance permeate flux in ultrafiltration using hollow fibre membranes. *J. Memb. Sci.*, 121: 175–184.
8. Cabassud, C., Laborie, S., and Laine, J.M. (1997) How slug flow can improve ultrafiltration flux in organic hollow fibres. *J. Memb. Sci.*, 128: 93–102.
9. Mercier, M., Fonade, C., and Lafforgue-Delorme, C. (1997) How slug flow can enhance the ultrafiltration flux in mineral tubular membranes. *J. Memb. Sci.*, 128: 103–109.
10. Cui, Z.F. and Wright, K.I.T. (1994) Gas-liquid two-phase cross-flow ultrafiltration of BSA and dextran solutions. *J. Memb. Sci.*, 90: 183–191.
11. Mercier-Bonin, M., Lagane, C., and Fonade, C. (2000) Influence of a gas/liquid two-phase flow on the ultrafiltration and microfilatration performances: case of a ceramic flat sheet membrane. *J. Memb. Sci.*, 180: 93–104.
12. Cui, Z.F., Chang, S., and Fane, A.G. (2003) The use of gas bubbling to enhance membrane processes–A review. *J. Memb. Sci.*, 221: 1–27.
13. Taha, T. and Cui, Z.F. (2002) CFD modelling of gas-sparged ultrafiltration in tubular membranes. *J. Memb. Sci.*, 210: 13–21.
14. Ndinisa, N.V., Wiley, D.E., and Fletcher, D.F. (2005) Computational fluid dynamics simulations of Taylor bubbles in tubular membranes—Model validation and application to laminar flow systems. *Chem. Eng. Res. & Design*, 83 (A): 40–49.

15. Ndinisa, N.V., Fane, A.G., and Wiley, D.E. (2006) Fouling control in a submerged flat sheet membrane system: Part I—Bubbling and hydrodynamic effects. *Sep. Sci. & Technol.*, 41 (7): 1383–1409.
16. Wu, M. and Gharib, M. (2002) Experimental studies on the shape and path of small air bubbles rising in clean water. *Phys. of Fluids*, 14: 49–57.
17. Sato, Y. and Sekoguchi, K. (1975) Liquid velocity distribution in two-phase bubbly flow. *Intl. J. Multiphase Flow*, 2: 79–91.
18. Lopez de Bertodano, M.A. (1992) Turbulent bubbly two-phase flow in a triangular duct. Ph.D. Thesis, (Nuclear Engineering), Rensselaer Polytechnic Institute: New York.
19. Cho, B.D. (2002) Treatment of high strength wastewater using membrane bioreactors, Ph.D. Thesis, University of New South Wales: Sydney, Australia.
20. Clift, R., Grace, J.R., and Weber, M.E. (1978) *Bubbles, drops and particles*. Academic Press: New York.
21. Valencia, A., Cordova, M., and Ortega, J. (2002) Numerical simulation of gas bubbles formation at a submerged orifice in a liquid. *Intl. Comm. Heat and Mass Transfer*, 29: 821–832.
22. Le-Clech, P., Alvarez-Vazquez, H., Jefferson, B., and Judd, S. (2003) Fluid hydrodynamics in submerged and sidestream membrane bioreactors. *Water. Sci. Technol.*, 48: 113–118.
23. Beek, W.J. and Muttzall, K.M.K. (1975) *Transport Phenomena*. Wiley: London.
24. Vitankar, V.S., Dhotre, M.T., and Joshi, J.B. (2002) A low Reynolds number k-ε model for the prediction of flow pattern and pressure drop in bubble columns reactors. *Chem. Eng. Sci.*, 57: 3235–3244.
25. Pfleger, D. and Becker, S. (2001) Modelling and simulation of the dynamic flow behaviour in a bubble column. *Chem. Eng. Sci.*, 56: 1737–1749.
26. Buwa, V.V. and Ranade, V.V. (2002) Dynamics of gas-liquid flow in a rectangular bubble column: experiments and single/multi-group CFD simulations. *Chem. Eng. Sci.*, 57: 4715–4726.
27. Delnoij, E., Kuipers, J.A.M., and Swaaij, W.P.M. (1997) Computational fluid dynamics applied to gas-liquid contactors. *Chem. Eng. Sci.*, 52: 3623–3631.
28. Kuwagi, K., Kusu, S., and Ozoe, H. (2000) Transient three-dimensional numerical analyses of shallow bubble column. *Chem. Eng. Sci*, 78: 5–17.
29. Jakobsen, H.A., Sannaes, B.H., Grevskott, S., and Svendsen, H.F. (1997) Modelling of vertical bubble-driven flow. *Ind. Eng. Chem. Res.*, 36: 4052–4064.
30. Lapin, A. and Lubbert, A. (1994a) Numerical simulation of the dynamics of two phase gas-liquid flows in bubble columns. *Chem. Eng. Sci.*, 49: 3661–3675.
31. Buwa, V.V. and Ranade, V.V. (2001) Dynamics of gas-liquid flow in 2-D bubble columns: Influence of sparger design, column geometry and physical properties. Proc. Intl. Conference on Multiphase flows. New Orleans, USA, .
32. Cui, Z.F. and Wright, K.I.T. (1996) Flux enhancement with gas sparging in downwards crossflow ultrafiltration: performance and mechanism. *J. Memb. Sci.*, 117: 109–116.
33. Cabassud, C. and Ducom, G. (2001) Air sparging in flat sheet nanofiltration membranes: effect on cake deposit and on concentration polarization. 6th World Congress of Chemical Engineering. Melbourne, Australia, September, 23–27.
34. Mercier-Bonin, M., Maranges, C., Lafforgue, C., Fonade, C., and Line, A. (2000) Hydrodynamics of slug flow applied to cross-flow filtration in narrow tubes. *AIChE. J.*, 46: 476–484.

35. Mercier, M., Fonade, C., and Lafforgue-Delorme, C. (1995) Influence of the flow regime on the efficiency of a gas-liquid two-phase medium filtration. *Biotech Techniques*, 9: 853–862.
36. Churchouse, S. and Wildgoose, D. (1998) Membrane bioreactor progress from the laboratory scale to full-scale use. *Memb. Technol.*, 111: 4–11.
37. Torvik, R. and Svendsen, H.F. (1990) Modelling of slurry reactors: A fundamental approach. *Chem. Eng. Sci.*, 45: 2325–2338.
38. Wicaksana, F., Fane, A.G., and Chen, V. (2006) Fibre movement induced by bubbling using submerged hollow fibres. *J. Memb. Sci.*, 271: 186–197.
39. Belfort, G. (1988) Membrane modules: comparison of different configurations using fluid mechanics. *J. Memb. Sci.*, 35: 245–258.